Bisphenol A Polycarbonate: Entanglement Analysis from Coarse-Grained MD Simulations

S. León,[†,‡] N. van der Vegt,[†] L. Delle Site,[†] and K. Kremer*[,†]

Max-Planck-Institute for Polymer Research, P.O. Box 3148, D-55021 Mainz, Germany, and Departamento de Ingeniería Química, Universidad Politécnica de Madrid, José Gutiérrez Abascal 2, E-28006 Madrid, Spain

Received May 5, 2005; Revised Manuscript Received July 21, 2005

ABSTRACT: Simulation data are presented for a coarse-grained model of polycarbonate (BPA-PC), which allow for a detailed comparison of different ways to study the chain dynamics and predict the entanglement molecular weight. Most of the standard experimental quantities are determined for the very same set of systems and thus provide an opportunity for a detailed comparison of data far beyond typical experiments or simulations. By employing a suitably coarse-grained model, which still contains the essentials of the BPA-PC structure, simulation times compared to atomistic simulations could be extended by several orders of magnitude, reaching well into the characteristic experimental regime. We find that a recently developed topological entanglement analysis compares well with a direct determination of the modulus from simulations as with experiments on well-characterized samples. This confirms the extraordinarily small value of the entanglement molecular weight on M_e between 1200 and 1400 corresponding to N_e close to 5.

I. Introduction

Dynamical, rheological, and mechanical properties of polymer melts (and glasses) play a central role in many applications of polymeric systems. They are crucial for processing as well as for final material properties. Such material properties not only are of mechanical nature but also can be related e.g. to the optical quality of a compact disk material, etc. All this originates from different physics and chemistry sources based on the local chemical structure as well as the overall size and topology of the specific polymer system. One such characteristic quantity, if not the central one, is the entanglement molecular weight M_e or the corresponding number of chemical repeat units N_e, which typically is determined from the plateau modulus $G^0 \propto N_e^{-1}$ of long chain polymer melts. N_e marks the characteristic chain length, where the transition from the short-chain Rouse-like to the long-chain reptation-like behavior occurs.[1] For short chains their dynamics is well described by a Langevin dynamics of a single chain, where all the complicated interactions with the surrounding chains are accounted for by a friction coefficient ζ of the beads. This leads to a chain diffusion constant of $D \propto N^{-1}$, N being the chain length, and a melt viscosity $\eta \propto N$ and a vanishing plateau modulus. For longer chains this does not hold anymore. The fact that the chains can slide along but not through each other becomes dominant and leads to a completely different dynamical behavior. Within the, by now well accepted, reptation theory[1−3] the characteristic chain length N_e for the crossover is related to the tube diameter d_T. The tube is a measure for the dynamical confinement a given chain experiences by all the other surrounding chains, in a way that a melt chain of length N_e just fits in the diameter of the reptation tube. Within this scheme the dominant relaxation mechanism is the curvelinear diffusion of the chains out of the original tube, which itself follows the coarse-grained contour of the original chain. Because of this link, N_e can be determined by rather different methods. Besides the original approach via the plateau modulus G^0, direct measurements of the mean-square displacements, of the diffusion constant, and of the intermediate dynamic scattering function have been performed. While the first measures a dynamic response of the system, the latter three are more closely related to the spatial dynamic confinement of the overall motion, as will be discussed below. Since all these different measurements look at different quantities, which are not linked via exact theoretical relations but rather involve different approximations, it is not surprising that one finds different results for N_e or M_e.[4,5] Because of its general importance for our understanding of the viscoelastic properties of polymers, there has been a great deal of effort to provide a better understanding of what an entanglement is.[6,7,9,10] In a recent numerical analysis of different coarse-grained polymer models and a reanalysis of many experimental data a topological analysis was presented, which for the first time directly linked the conformation of the chains quantitatively to the backbone of the tube, the primitive path, and thus to N_e. This let to a quantitative prediction of the modulus G^0 based on the chain conformations and compared very well with other simulations as well as with experiments[7,8] for systems as different as a freely jointed bead−spring chains or polyethylene or BPA-PC.

Typically N_e, as reported in the literature, varies for polymer melts between about 100 (polyethylene) and 180 (polystyrene) repeat units.[6] In this context polycarbonate (bisphenol A polycarbonate, BPA-PC) (Figure 1) is a rather special case. BPA-PC is a commercially very important polymer with many valued properties such as high impact strength, ductility combined with a high glass transition temperature (around 420 K), electrical insulation, and optical transparency. As a consequence,

† Max-Planck-Institute for Polymer Research.
‡ Universidad Politécnica de Madrid.
* Corresponding author. E-mail: kremer@mpip-mainz.mpg.de.

10.1021/ma050943m CCC: $30.25
Published on Web 08/24/2005

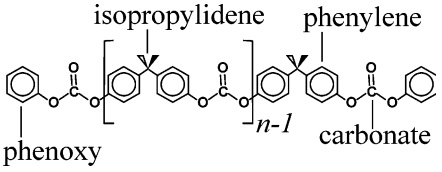

Figure 1. Schematic representation of the structure of bisphenol A polycarbonate. The relevant comonomeric groups are labeled.

BPA-PC is by far the most utilized and intensively studied variety of polycarbonate (applications include electrical distribution boxes, automotive parts, airplane windows, high-quality optical equipment such as CDs and lenses). Of particular interest in the present context is its unusually small entanglement length N_e, which is reported to be between 5 and 11 repeat units,[6,11−17] where the more recent results on well-characterized samples tend toward the smaller numbers. Even though the BPA-PC monomer is a rather extended object and one might very well compare one such unit to effectively a few PE or PS repeat units, the actual value of N_e is still very small. It is the purpose of the present work to shed more light on this fact and on the different ways of determining N_e and provide a rather complete analysis of that particular interesting system by computer simulation. To do so, we perform large-scale molecular dynamics simulations, employing a specially adapted coarse-grained model, which on one hand allows for very efficient large time scale simulations and on the other hand keeps enough of the molecular details in order to provide specific results for BPA-PC. By this the effective time scale, which can be reached by simulating such a particle based and topology conserving model, of a specific polymer is extended to almost 10^{-4} s, several orders of magnitude more than any other simulation study of that kind so far. The simulations were all performed at a temperature of 570 K, a typical process temperature for BPA-PC. However, employing a time scaling due to the known Vogel−Fulcher behavior of BPA-PC, which describes the slowing down of the dynamics by cooling the system, predictions for other temperatures can be made as well.

The paper is organized as follows: first the methodology is described in some detail, and then standard experimental procedures are "performed" on our equilibrated, absolutely monodisperse "samples". A detailed comparison of these results with a variety of experiments and a short discussion conclude the paper.

II. Methodology

First, the coarse-graining procedure is shortly reviewed, and then the setup and equilibration of the melts are discussed.

A. The Coarse-Grained Bead−Spring Model of BPA-PC. Coarse-graining procedures are aimed to drastically reduce the number of degrees of freedom while keeping the description of macroscopic properties at the necessary level of accuracy and detail. What level is needed depends on the problem considered. For the study of long time dynamics of polymer melts, usually the most simple models are employed because of the slow intrinsic dynamics and the resulting long simulation times.[18−20] This excellent computational efficiency is obtained by the price of loosing the direct link to a specific chemical system. As long as one is only interested in generic properties of polymers, this is the optimal choice and led to many important results. If one wants to study a specific system, this however is not sufficient, and a closer link to the underlying chemical structure is needed. Examples are the determination of the tube diameter d_T itself and thus N_e, as well as the molecular motion on scales up to $O(d_T)$ and in some cases beyond (depends on the level of detail of the model employed). The model also should resemble closely the original structure in order to allow a mapping back onto an all-atom description. For polymers this can be achieved by mapping atomistic chains onto suitable bead−spring models. Because of the simplification introduced, the coarse-graining procedure allows to generate, with a reasonable computational effort, equilibrated melt conformations, which otherwise are rather difficult to obtain with an atomistic resolution. These then can be used to perform long time simulations to study dynamic phenomena. Previous studies on different polycarbonates (PC) showed that such an approach successfully reproduced variations in the dynamics of various chemical modifications of PC.[21]

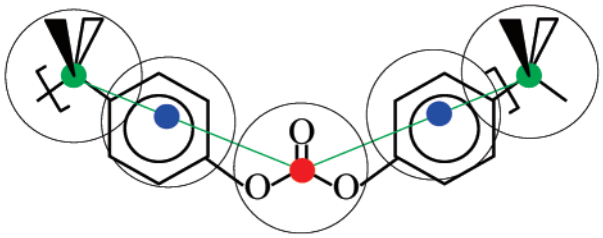

Figure 2. Schematic representation of the coarse-grained 4:1 scheme for BPA-PC. Each chemical repeat unit is represented by four beads, corresponding to the isopropylidene, carbonate, and the two phenylene groups. Because of the chain ends, a coarse-grained chain of a polymer of N repeat units contains $4N + 3$ spheres (cf. Figure 1).

For PC such coarse-graining procedures have been used to study a variety of short-chain properties. There, a so-called 4:1 mapping scheme turned out to be both accurate and computationally very efficient. Here we apply this to melts of long chains. In the 4:1 coarse-graining scheme for BPA-PC (Figure 2)[22] each chemical repeat unit is represented by four mapping points, which correspond to the carbonate, the isopropylidene, and the two phenylene subunits. The mapping points for carbonate and isopropylidene are taken as the backbone carbon atoms of each group, while for the phenylene subunits the mapping spheres do not correspond exactly to the position of the group, but lie in the straight line between the carbonate and isopropylidene beads (as explained next). All beads interact via intramolecular bond length and angle potentials, which are derived from a Boltzmann inversion of the atomistic distribution function obtained from isolated chains, whose potentials has been directly calculated by quantum chemical methods. This leads to a parametrization of the coarse-grained model without any fitting function (up to some smoothing of the distribution functions due to statistical scatter originating from the sampling; for more details see ref 21). The nonbonded excluded-volume interaction is taken into account by a soft purely repulsive potential.

The systems studied range from $M = 50$ chains of $N = 5$ repeat units (meaning 23×50 particles or beads, below N_e) to $M = 200$ chains of 120 repeat units (meaning 483×200 beads). Details including the chain extensions are given in Table 1.

Table 1. Chain Length N, Number of Chains M, Box Dimensions [Å], Mean-Square End-to-End Distance $\langle R_{e-e}^2 \rangle$ [Å²], and Mean-Square Radius of Gyration $\langle R_G^2 \rangle$ [Å²] for the Different Monodisperse BPA-PC Melts Considered in the Bulk Simulations[a]

N	$4N+3$	M	box dimension	$\langle R_{e-e}^2 \rangle$	$\langle R_G^2 \rangle$
5	23	50	48.8	1135 ± 300	164 ± 30
10	43	50	60.1	2270 ± 580	348 ± 60
15	63	100	86.0	3500 ± 750	550 ± 60
20	83	100	94.3	4630 ± 950	750 ± 65
30	123	100	107.5	7470 ± 1150	1120 ± 75
60	243	100	134.8	12800 ± 2000	2130 ± 100
120	483	200	213.6	24800 ± 2000	4000 ± 100

[a] Note that $\langle R_{e-e}^2 \rangle$ is always calculated between the first and the last bead of the chain; similarly, $\langle R_G^2 \rangle$ takes all the $4N+3$ beads into account.The large error bars are due to the still relatively small number of chains and sampling times, which for the longest chains do not fully reach the longest relaxation times.

Here we set the notation for the subsequent chapters. By N we will always denote the number of chemical repeat units of a polymer. For the simulation model this means that such a chain is represented by $4N+3$ beads, where the 3 beads come from the typical polycondensation process (cf. Figure 1). When quoting lower case "n", we will always consider the beads of the simulation model. The distinction between chemical repeat units and beads will be kept throughout the whole paper. Because of the expected small value for N_e, corrections due to the chain end beads can be important. It should be noted that the longest chains ($N = 120$) approximately correspond to 11−25 entanglement lengths, depending on the experimental value quoted for reference, thus ensuring that chains are long enough to properly display reptation behavior of melts.

Details: Bond Angles. Tabulated bond angle potentials $U_{CIC}(\theta)$ and $U_{ICI}(\theta)$ are employed for each carbonate−isopropylidene−carbonate (CIC) and isopropylidene−carbonate−isopropylidene (ICI) sequence. The probability distributions, $P_{CIC,ICI}(\theta)$, needed for the Boltzmann inversion, were generated via Metropolis Monte Carlo sampling of single atomistic random walk chain conformations in a vacuum. For details and how to avoid the problem of double counting interactions in this procedure, we refer to refs 21−23. θ is determined for the corresponding mapping points on the atomistic chain. The carbonate−phenylene−isopropylidene angles (centered at the phenylene) are enforced to 180° by a simple harmonic potential; in this way the corresponding mapping point is "decoupled" from the center of the respective atomistic group, thus excluding additional torsional degrees of freedom correlated to the angle at the carbonate group which would require the introduction of a complicated multibody potential in the model (see ref 22 for details). Because phenylene beads adjacent to the same isopropylidene, on both sides, can weakly overlap when represented as spheres, the excluded-volume interaction for these intramolecular phenylene−phenylene beads is turned off. No further torsion potentials are considered as the torsional barriers at the carbonate group (I−C−I−C torsion) for the coarse-grained model are smaller than k_BT. These constraints, in the form of bond angle potentials, ensure that the conformations sampled by the chain reflect, as much as possible, the statistics obtained from a (quantum-based) atomistic potential energy surface.

Distances. Distances between neighboring beads are enforced by harmonic spring potentials:

$$U_{bond}(r_{ij}) = \frac{1}{2} k_{ij} (r_{ij} - r_{ij}^0)^2 \quad (1)$$

Mean bond lengths r_{ij}^0 and standard deviations are 3.56 ± 0.04 Å for the carbonate−phenylene bond and 2.93 ± 0.04 Å for the isopropylidene−phenylene bond. They also are derived from the sampling of the original all-atom random walks.

All intrachain potentials have been directly obtained from a Boltzmann inversion of distribution functions at 570 K. Note that in this respect the "energies" within the classical potentials of the coarse-grained model contain energetic as well as entropic contributions. Thus, the simulation temperature in the usual Lennard-Jones units, which is set to one, corresponds to a real temperature of 570 K.

The excluded-volume nonbonded interactions are represented by a simple truncated repulsive 12−6 Lennard-Jones (WCA, Week−Chandler−Anderson) pair potential between spherical beads of size σ_i

$$U_{LJ}(r_{ij}) = \begin{cases} 4\epsilon\left[\left(\frac{\sigma_{ij}}{r_{ij}}\right)^{12} - \left(\frac{\sigma_{ij}}{r_{ij}}\right)^{6} + \frac{1}{4}\right] & r_{ij} < 2^{1/2}\sigma_{ij} \\ 0 & r_{ij} \geq 2^{1/6}\sigma_{ij} \end{cases} \quad (2)$$

where $\sigma_{ij} = {}^1/_2(\sigma_i + \sigma_j)$; ϵ is chosen as the unit of energy, which is set to k_BT. Bead sizes, σ_i, are computed by first calculating the gyration radii among atomic positions in each group and then scaling these radii such that the volume of the repeat unit, accounting for the overlaps of adjacent beads, is equal to the van der Waals volume per repeat unit of BPA-PC computed using an equation-of-state analysis.[24] The values for the bead size are 5.19 Å for isopropylidene, 3.49 Å for carbonate,[52] and 4.67 Å for phenylene. Taking a number density of $0.85\sigma^{-3}$ for the beads in the simulation, the mapping of the bond lengths and bead diameters onto the experimental mass density of 1.05 g/cm³,[21] the experimental value at 570 K, results in a conversion factor of

$$1\sigma = 4.41 \text{ Å} \quad (3)$$

Molecular dynamics (MD) simulations were performed using a procedure formally identical to that previously applied.[21,22] In MD the classical equations of motion are integrated numerically. The velocity-Verlet algorithm was used to integrate the particle equations of motion using a constant time step of 0.01τ, were τ is the unit of time in reduced Lennard-Jones units, which were used in most cases throughout the paper. A Langevin-type thermostat with friction $\Gamma = 0.5\tau^{-1}$ was used to keep the temperature which was set to 1.0.[25] The energy is measured in units of $k_BT = 1.0\epsilon$ corresponding to an experimental temperature of $T = 570$ K, a typical process temperature for BPA-PC, well above the glass transition temperature ($T_g \approx 420$ K).

Time Mapping. While the ratio of σ to Å is trivially given by the coarse-graining procedure itself, an absolute time mapping is lost since the time dependence of measured quantities is predominantly determined from bead−bead interactions across the sample (bead friction), rather than from the intramolecular coarse graining, which would define a renormalization of the fast oscillations along the backbone. Thus, the mapping of the simulation times requires some different procedure. One way would be to resort to a scheme set up by some earlier simulations,[21] where the viscosity η originating

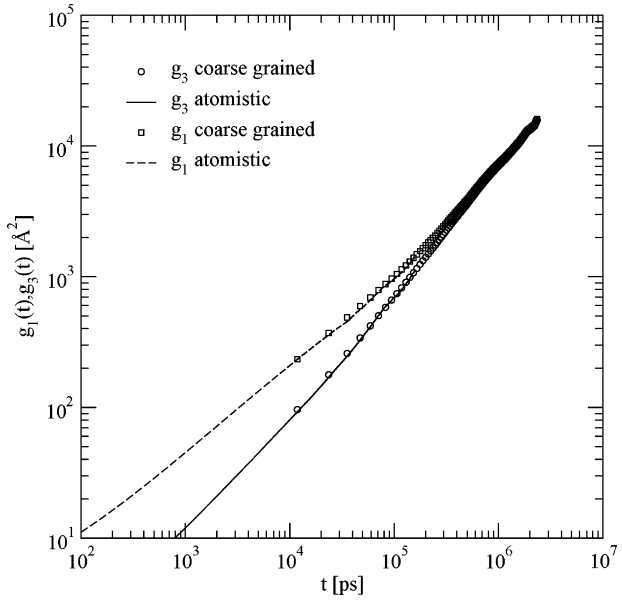

Figure 3. Mean-square displacements of the centers of mass and repeat units, $g_1(t)$, averaged over all repeat units or beads, respectively, for an $N = 5$ melt of 50 chains in an all-atom simulation and a bead−spring simulation, leading to the absolute time scaling of the coarse-grained bead−spring simulation.

from the diffusion constant D of short chains was compared to experimental values of η. This procedure, though giving a first estimate, bears a number of uncertainties. The most crucial one relates to the typically longer chains and the polydispersity of the experimental samples. Thus, the basic assumption of the Rouse model, which is used for that mapping, contains some poorly controlled approximations. The most clean, however also more expensive, way is to perform an all-atom and an equivalent coarse-grained simulation for a short time and then compare the displacements vs time. This provides an absolute time mapping. To do that, an all-atom system of 50 chains of 5 repeat units each was simulated at exactly the same density (1.05 g/cm^3), temperature (570 K), and system size as the corresponding coarse-grained system. The force field developed in ref 38 for BPA-PC was employed, and the simulations were performed with the GROMACS package. On the coarse-grained side $N = 5$ is the smallest chain length considered. The all-atom simulations ran with a time step of $\delta t = 2$ fs and were performed for a total time of 160 ns. This leads to an averaged mean-square displacement of the chains of up to 1400 Å^2, about $8 - 9\langle R_G^2(N = 5)\rangle$! This is sufficient to obtain a significant overlap in time and displacement with the coarse-grained simulations of the same system, as Figure 3 shows. By fitting the time of the coarse-grained simulation to the all-atom simulation to optimal overlap, one arrives at a time mapping of

$$1\tau \approx 2.6 \times 10^{-11}\,\mathrm{s} \tag{4}$$

Note that for this mapping it is important to reach simulations times on the all-atom level, which correspond to displacements larger than the characteristic size of the repeat unit. Thus, the longest runs, which we present in this paper, reach averaging times of up to about 5×10^{-5} s. This is much more than any other particle based simulation of a specific polymer before. However, for rheometers this still is difficult to reach, and also the temperature of $T = 570$ K, which is the typical process temperature, is very high for experiments. However, taking into account that the chain conformations only very weakly depend on temperature[21,27] and following the known Vogel−Fulcher−Tamann behavior of BPA-PC, as it is used in experimental time temperature data analysis as well, we can extend our predictions to much longer times. Taking the characteristic temperature dependence of the viscosity, where the exponential describes the slowing down of the dynamics

$$\eta(T) = \eta_0 \exp(A_0/(T - T_{VF}) \tag{5}$$

the resulting time factor is also given by the same exponential. Using this, we can estimate the time mapping for different temperatures at least in an approximate way. With $A_0 \simeq 1000$ K and $T_{VF} \simeq 387$ K, we arrive at $1\tau \simeq 7.5 \times 10^{-10}$ s for $T = 500$ K and at $1\tau \simeq 8.3 \times 10^{-7}$ s for $T = 450$ K. Note that the glass transition temperature of BPA-PC is at $T = 420$ K. Comparing this now to our longest simulations, we reach times of up to 2×10^{-3} s for $T = 500$ K and even the much longer time of about 2 s for $T = 450$ K. Though this contains some uncertainty, which is mainly due to some deviations from the ideal Vogel−Fulcher−Tamann behavior and some uncertainties in determining A_0 and T_{VF} precisely, the subsequent simulations present a particle-based simulations analysis which reaches times deep into the accessible experimental regime and with the extrapolation to lower temperatures even up to times easily observed by the eye! Because experiments probably are not made at the current simulation temperature and also because the time scaling is, unlike the length scaling, strongly temperature dependent, we in the following sections mostly give the time in units of τ. For the reader it is, however, easy to transform this into real time units even at a desired temperature different from $T = 570$ K, keeping the above notes of caution in mind.

B. Setup and Equilibration. Equilibration of long chains polymer melts poses a special problem, since the overall relaxation time is often of the order of the whole run time. Samples are characterized by specifying the number of chains, of beads per chain, and system density. Chains were first randomly placed in a box and grown according to the bond length and bond angle probability constraints (for details, see ref 21) in a way that the average end-to-end distance and radius of gyration of the chains equal the expected values, which is known from earlier simulations as well as, to some extent, experiments. A 5000-step "push-off" integration is then performed to remove bead−bead overlaps.[26] During this stage, all particles interact via a radially shifted WCA repulsive particle−particle pair potential

$$U_{rs}(r_{ij}) = \begin{cases} 4\epsilon\left[\left(\frac{\sigma_{ij}}{r_{ij} + 2^{1/6}\sigma_{ij}b(t)}\right)^{12} - \left(\frac{\sigma_{ij}}{r_{ij} + 2^{1/6}\sigma_{ij}b(t)}\right)^{6} + \frac{1}{4}\right] & [r_{ij} + 2^{1/6}\sigma_{ij}b(t)] < 2^{1/6}\sigma_{ij} \\ 0 & [r_{ij} + 2^{1/6}\sigma_{ij}b(t)] \geq 2^{1/6}\sigma_{ij} \end{cases} \tag{6}$$

where $\sigma_{ij} = {}^1/_2(\sigma_i + \sigma_j)$ and $\epsilon = 1\ k_BT$. The radial shift term $b(t)$ decays linearly from unity to zero over the duration of the push-off stage:

$$b(t) = \frac{t_f - t}{t_f - t_i} \tag{7}$$

Here, t_i and t_f are the initial and final time values of the push-off stage, respectively. During this time the form factor of the chain was controlled to make sure that typical artifacts of a too fast pushoff did not occur. An improved scheme, where also the typical problems which might occur are discussed, is reported in Auhl et al.[28] After the push-off phase, the full MD simulations are performed for times sufficient to equilibrate the chains in the melt. As a good working definition, equilibration and good averaging are achieved when the mean-square displacement of chain centers of mass significantly exceeds the chain mean-squared radius of gyration. This can only be reached for the shorter chains ($4N + 3 \leq 123$). For the larger systems, however, this time is too large. Because of the self-similar structure of the chains, internal distances in the shorter, but already long enough, chains to display asymptotic behavior, e.g. $N = 30$, have the same value as in longer chains. Therefore, average internal distances and simultaneously the self-similar structure are monitored via the form factor (see below) to ensure proper equilibration and averaging here as well. Additional simulations on melts with "chain lengths" of $N = 1$ and 2 were used in some cases for comparison for dynamic properties.

III. Results and Discussion

We first focus on the static properties of the melts to ensure that our systems are (a) well characterized and that (b) the statistical properties compare well to a monodisperse PC melt at $T = 570$ K. For this typical lengths are given in [Å] and, where appropriate, in [σ]. After that the characteristic short time and/or short chain length Rouse dynamics is analyzed, including a modified version of the time−temperature superposition to account for the chain length dependent bead friction (or in experimental terms to account for the differences in distance from the glass transition temperature).[3] The combined results are then used to determine the entanglement length N_e following five different approaches: (i) from the mean-square displacements, $N_{e,msd}$; (ii) from the scaling of the diffusion coefficient D of the chains, $N_{e,D}$; (iii) from the dynamic structure factor $S(q,t)$ of the chains, $N_{e,sf}$; (iv) from the plateau modulus G_N^0 of the melts, $N_{e,pm}$; (v) from a primitive path analysis,[7] $N_{e,pp}$.

A. Static Properties. Chain Dimensions. Table 1 and Figure 4 report the mean-square end-to-end distance $\langle R_{e-e}^2 \rangle$ and mean-square radius of gyration $\langle R_G^2 \rangle$ for the different melts. The results show that both $\langle R_{e-e}^2 \rangle$ and $\langle R_G^2 \rangle$ linearly scale with the chain length N, and the ratio $\langle R_{e-e}^2 \rangle / \langle R_G^2 \rangle$ is close to 6, as expected for random walk statistics, which the chain in a melt should follow. For the ratio $\langle R_{e-e}^2 \rangle / N$ we obtain 215 ± 10 Å^2, after considering the fact that the chains contain $4N + 3$ beads, and for $\langle R_G^2 \rangle / N$ we obtain a value of 35 ± 1 Å^2 for the longer chains ($N \geq 15$). This compares reasonably well with the results of previous simulations[21,22,27] ($\langle R_G^2 \rangle / N \simeq 35.5$ Å^2 at $T = 600$ K[53]) and with the experimental values of 37.33 and 36.01 Å^2, obtained from neutron scattering[29] and viscosimetric data[30] (where an extrapolation from solutions to melt density is needed) respectively, both at a temperature of 300 K. (A slight increase of this quantity is expected for a lower temperature due to the temperature dependence of the trans−cis ratio at the carbonate group.)

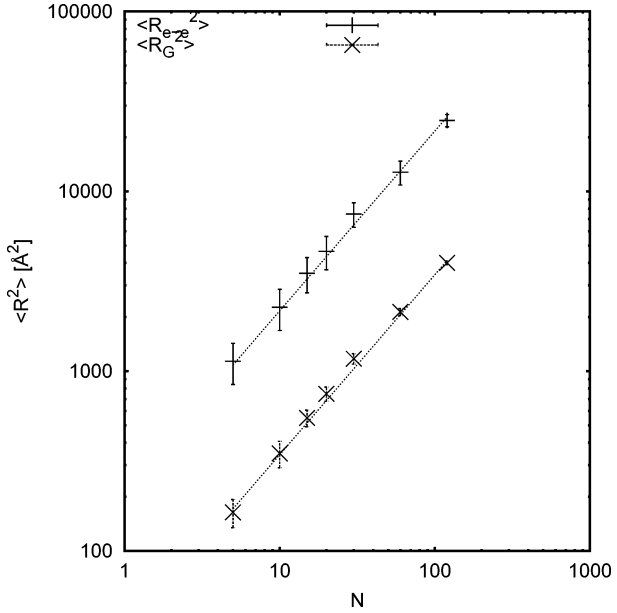

Figure 4. Mean-squared end-to-end distance $\langle R_{e-e}^2 \rangle$ and radius of gyration $\langle R_G^2 \rangle$ as a function of the chain length N for the monodisperse melts of BPA-PC. Dotted lines indicate the expected linear dependence with N for both $\langle R_{e-e}^2 \rangle$ and $\langle R_G^2 \rangle$, with a ratio of $\langle R_{e-e}^2 \rangle / \langle R_G^2 \rangle = 6.2$ close to the optimal value of 6; see Table 1 for details.

Internal Correlations. More insight into the overall static properties is provided by the single-chain form factor

$$S(q) = \frac{1}{4N+3} \left\langle \left| \sum_{j=1}^{4N+3} \exp(i\mathbf{q}\cdot\mathbf{r}_j) \right|^2 \right\rangle_{|\mathbf{q}|} \tag{8}$$

$\mathbf{r}_j$ being the position of "scattering bead" j of the chain (note each repeat unit contains 4 "beads"). The averaging here is over conformations as well as orientations of the q-vector. According to the statistics of Gaussian chains, the form factor $S(q)$ should scale as q^{-2} for $2\pi/R_G \ll q \ll 2\pi/l_K$, l_K being the Kuhn length. The single chain form factor for the BPA-PC melts is displayed in Figure 5. The results for BPA-PC indicate that this dependence is obtained up to a value of $q \approx 0.2$ Å^{-1}, corresponding to about 30 Å, after which the local correlations originating from the shape of the beads and the possible bond angles show up. These particular conformational properties of the BPA-PC chains can be illustrated by a series of banana-like rigid segments centered at the isopropylidene, connected by rather flexible joints at the carbonate units, which have a typical separation of about 11 Å. This kind of conformation is reflected in the probability distribution function of the distance for next-neighbor carbonate−carbonate pairs and next-neighbor isopropylidene−isopropylidene pairs, as shown in Figure 6. Both distributions present localized populations at distances close to 10 and 11 Å, respectively. In particular, the distribution function for the isopropylidene pairs displays two peaks, corresponding to the cis−trans and trans−trans populations at the carbonate group. The percentage obtained for the cis−trans conformation is about 36%, which again compares well with previous simulations.[21,27] The resulting rigidity of a chain is also well described by the

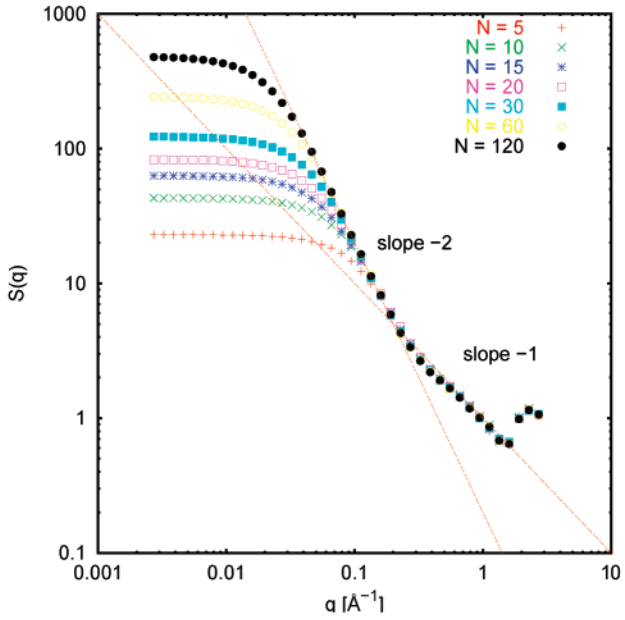

Figure 5. Single chain form factor $S(q)$ for the BPA-PC melts. Dotted lines indicate the dependence of q^{-2} and q^{-1}. Note that due to the mapping scheme, $S(q=0) = 4N + 3$. The scattering amplitude of each bead is identical and set to 1.

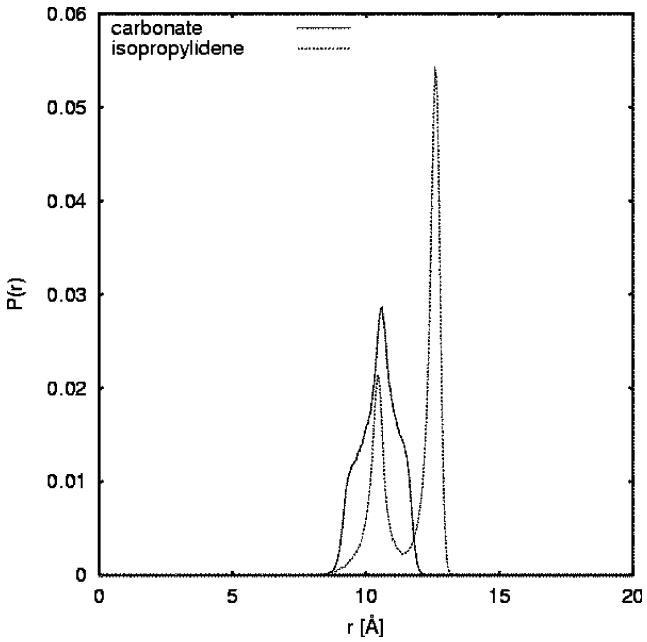

Figure 6. Probability distribution functions for coarse-grained distance between next neighbors carbonate−carbonate and isopropylidene−isopropylidene pairs along the chains, for the melt with $N = 120$ repeat units. Similar plots are obtained for the other melts. The peak around 10 Å for carbonate−carbonate pairs indicates the conformational nature of BPA-PC chains, constituted by banana-like-shaped rigid segments centered at the isopropylidene units. The two peaks in the isopropylidene−isopropylidene distribution function correspond to the cis−trans and trans−trans conformations of the carbonate group.

persistence length l_p, with $2l_p = l_K$ for random walks. l_p can be obtained from the bond correlation function along the backbone (see Figure 7) by fitting to the expression

$$\langle \mathbf{u}(n)\cdot\mathbf{u}(n+j)\rangle \propto e^{-jl_0/l_p} \qquad (9)$$

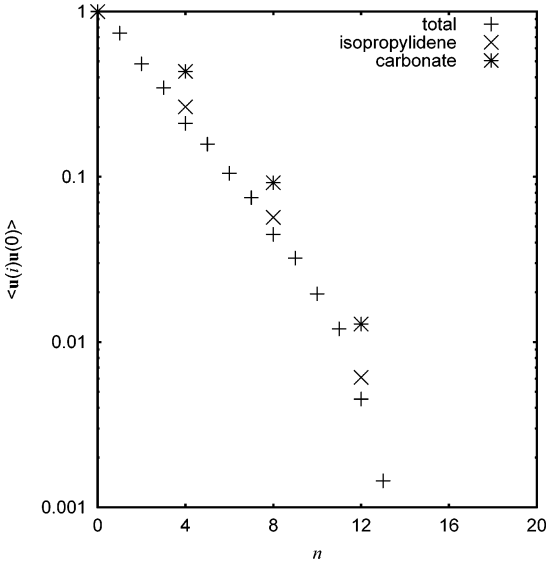

Figure 7. Normalized bond correlation function along the chain backbone used in the calculation of the persistence length for the $N = 120$ melt. Note that the index n denotes bonds between beads, not chemical repeat units. Analogous functions for more coarse-grained "bonds", which connect either subsequent isopropylidenes or carbonates, are also shown. In the correlation function for the carbonate−carbonate bonds displays the specific short-range deviation from the asymptotic structure due to the shape of the rigid repeat units, while the isopropylidene−ispropylidene bond already contains a flexible joint.

where $\mathbf{u}(n)$ is the (bond) vector connecting two adjacent beads n and $n + 1$ and l_0 the average bond length. The value obtained for l_p corresponds to about 3 beads in the 4:1 representation and corresponds to about 0.7 repeat units (since each repeat unit contains four beads). This value can be interpreted as a consequence of the flexibility of the torsions at the carbonate groups together with the overall banana-like shape of the monomer. Accordingly, a similar value for l_p is obtained (in terms of repeat units) when a vector connecting the isopropylidene groups of two adjacent monomers (i.e., representing a whole repeat unit) is considered. On the other hand, a value close to 1.0 bonds is obtained when the vector connects carbonate groups, showing the rigidity of such a segment, in particular due to the stiff angles at the isopropylidene group. In all cases of the different ways to define a bond l_0 in order to account for the internal structure of the PC monomer the relation of $l_K = 2l_p$, which holds exactly for random walks (note that $\langle R^2(N)\rangle = l_K l_0 N$), is surprisingly well reproduced. The crossover in the decay of the chain form factor $S(q)$ reasonably well fits into this picture. It should however be kept in mind that the data are discussed in terms of statistical mechanics of random walks down to length scales, where details of the chemical structure already are expected to be relevant. Thus, an absolute quantitative agreement cannot be expected.

Correlation Hole. Besides the internal structure and the bead packing, the overall chain packing is relevant and leads to the characteristic correlation hole of the chains. Figure 8 shows this as it is given by the normalized radial distribution function of chain beads from other chains as a function of distance from the center of mass of a given test chain. It can be seen that such a hole extends over a distance that roughly corresponds to the average radius of gyration of the

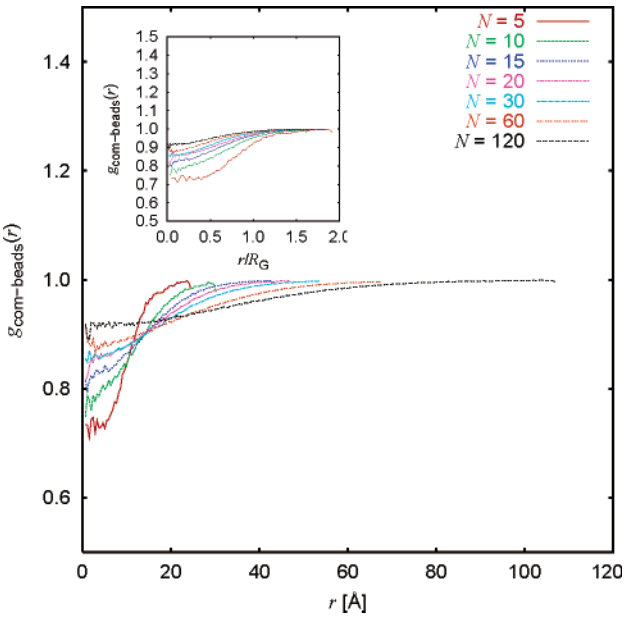

Figure 8. Intermolecular center of mass−individual bead radial distribution function vs the distance for the BPA-PC melts. The inset shows same data plotted vs the scaled r/R_G. The fluctuations at short distances r are due to the small sampling volume $4\pi r^2\,dr$.

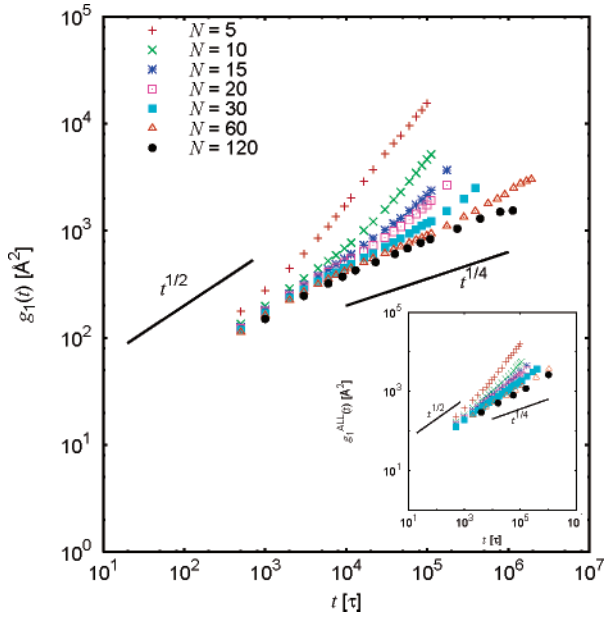

Figure 9. Average mean-squared displacement $g_1(t)$ for the inner individual beads of each chain. Solid lines indicate the power law dependence of 1/2 and 1/4. In the inset, the same function averaged over all beads of each chain is displayed.

chains. On the other hand, the correlation hole becomes deeper for the shorter chain lengths, indicating that the degree of interpenetration of the chains increases with the chain length, since the volume of a chain is shared by $O(N^{1/2})$ other chains. The other chains form a soft cage in the chain liquid producing the initial subdiffusive behavior of the center of mass motion (see below). For polymer melts this results in a characteristic $t^{0.8}$ power law for the mean-square displacement of the center of mass on short time and length scales.[20,31,32]

B. Mean-Square Displacements. The dynamics of the different simulated systems is summarized in

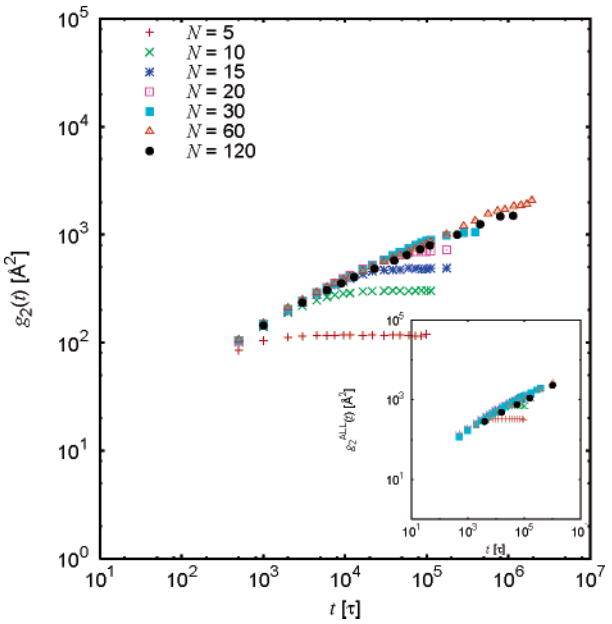

Figure 10. Average mean-squared displacement $g_2(t)$ for the inner individual beads relative to the center of mass of each chain. In the inset, the same function for all the beads of each chain is displayed.

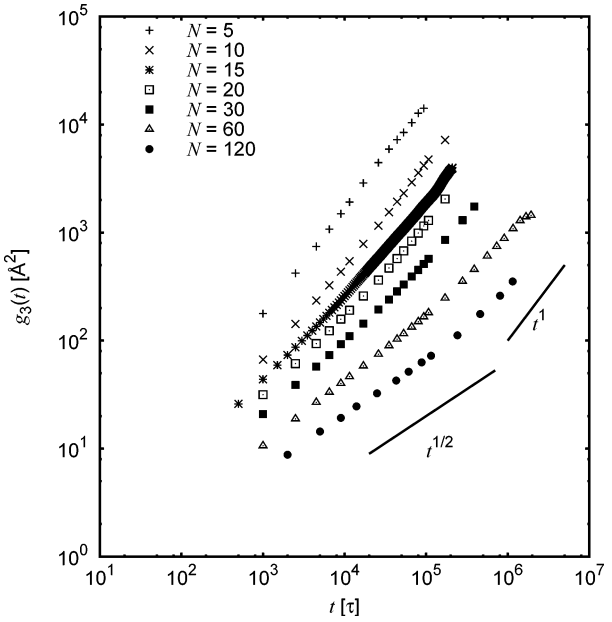

Figure 11. Average mean-squared displacement $g_3(t)$ for the center of mass of each chain. Solid line indicates the power law dependence of $t^{1/2}$ and t^1.

Figures 9, 10, and 11, showing respectively the mean-square displacements (msd) g_1, g_2, and g_3:

$$g_1(t) = \langle \Delta r^2(t) \rangle = \langle |\mathbf{r}_i(t) - \mathbf{r}_i(0)|^2 \rangle \qquad (10)$$

represents the msd for the individual beads of each chain

$$g_2(t) = \langle |\mathbf{r}_i(t) - \mathbf{r}^{cm}(t) - \mathbf{r}_i(0) + \mathbf{r}^{cm}(0)|^2 \rangle \qquad (11)$$

represents the msd of the individual beads relative to the chain's center of mass r^{cm}, and

$$g_3(t) = \langle |\mathbf{r}^{cm}(t) - \mathbf{r}^{cm}(0)|^2 \rangle \qquad (12)$$

represents the msd of chain centers of mass. The brackets denote an averaging over the individual trajectories of all the chains in the system. For g_1 and g_3 the center-of-mass motion of the whole system originating from the Langevin thermostat has been removed.[19] The crossing point between g_2 and g_3 is a first measure of the equilibration time since it roughly indicates the average time required for the beads to diffuse a distance of the chains radius of gyration. Both g_1 and g_2 have been computed considering the inner eight (four for the chain length $N = 5$) beads (two repeat units) of every chain to avoid chain end effects; for comparison, the same functions obtained considering all the beads of each chain are shown in the insets in Figures 9 and 10. Here we give the distances in Å^2 in order to allow for a direct comparison to the experimentally accessible values of R_G^2. A detailed test of the expected asymptotic values for $g_2 \rightarrow \infty$ can be found in Paul et al.[31,34]

For different (time) regimes the reptation model predicts the following power laws for g_1:[1,2]

$$g_1(t) \sim \begin{cases} t^{1/2} & t \le \tau_e \propto {N_e}^2 \\ t^{1/4} & \tau_e \le t \le \tau_R = \tau_e N^2/{N_e}^2 \\ t^{1/2} & \tau_R \le t \le \tau_d \propto N^3/{N_e}^2 \\ t & \tau_d \le t \end{cases} \qquad (13)$$

while for g_3 the predicted power laws are

$$g_3(t) \sim \begin{cases} t & t \le \tau_e \\ t^{1/2} & \tau_e \le t \le \tau_R \\ t & \tau_R \le t \end{cases} \qquad (14)$$

where τ_e is the entanglement time, τ_R the Rouse time, and τ_d the disentanglement time.[1] Results for g_1 displayed in Figure 9 show that for chain lengths of $15 \le N \le 20$ repeat units (i.e., relatively short) already a significant deviation from the $t^{1/2}$ power is observed, a first indication of the unusually short entanglement length of BPA-PC. Most remarkably, for the longest chains, the 1/4 power law (eq 13) is almost reached, another indication of the very small entanglement molecular weight (in such studies usually the value of the time exponent does not fall below 0.3[18,20,31]). More evidence in this direction is obtained for g_3 from Figure 11; here we observe 1/2 power law for intermediate times (eq 14). Besides this the correlation hole induced reduction of $g_3(t)$ from the Rouse-like t^1 to the $t^{0.8}$ is perfectly reproduced.

For a more complete analysis one has to take into account that the bead friction ξ for the Langevin dynamics of the chain, which results from the bead−bead interaction, is chain length dependent. To a good first approximation $\zeta(N) = \zeta(1 - a/N)$ with a close to N_e. This is due to the fact that the glass transition temperature changes with the chain length for short chains.[3] Though relatively far away from the glass transition temperature $T_g \simeq 420$ K this is relevant here, especially for the shorter chains. In the present simulation scheme with purely repulsive nonbonded potentials this effect would be even more pronounced in a constant pressure simulation. Though similar to experiment, the actual shift in $\zeta(N)$ might be somewhat different than in a corresponding experiment on BPA-PC. This is reflected in Figure 12, where the ratio $g_1/t^{1/2}$ is plotted as a function of time. In the region corresponding to the Rouse regime (initial $t^{1/2}$ regime of $g_1(t)$, thus $t < \tau_e$), where the slope is zero, this ratio should be proportional to $\zeta^{-1}(N)$. Figure 12 shows this dependency. As a consequence, the mean-square displacements should be corrected using a simplified time−temperature superposition principle, similar to what is applied in rheology experiments.[3,33] This is done by rescaling the time (the new scaled values will be referred as t^* in the text and in units τ^*) in such a way that the mean-square displacements of the inner beads of all chains coincide in the time window which corresponds to the Rouse regime (approximately at 1000τ). Time shifts used to rescale the time are summarized in Table 2. Note that this does not affect the time mapping given before, as this is for the original time evolvement of the system. Since all displacements now are normalized to the $N = 60$ system, the previous time mapping in units of t^* holds for that system quantitatively, while for the other systems the inverse shift factor of Table 2 has to be applied. Results obtained by applying the time−temperature superposition principle are shown in Figures 13 and 14 for g_1 and g_3, respectively. For g_1, the prefactor in the power laws for times shorter than the Rouse time τ_R depend on parameters like the tube diameter d_T or the effective bead friction, but not on the chain length N. Accordingly, in Figure 13, the mean-square displacements g_1 coincide for all the melts at short times. For g_3, the corresponding prefactor of the power laws in the Rouse regime in addition is expected to display the Rouse N^{-1} scaling, so the curves should

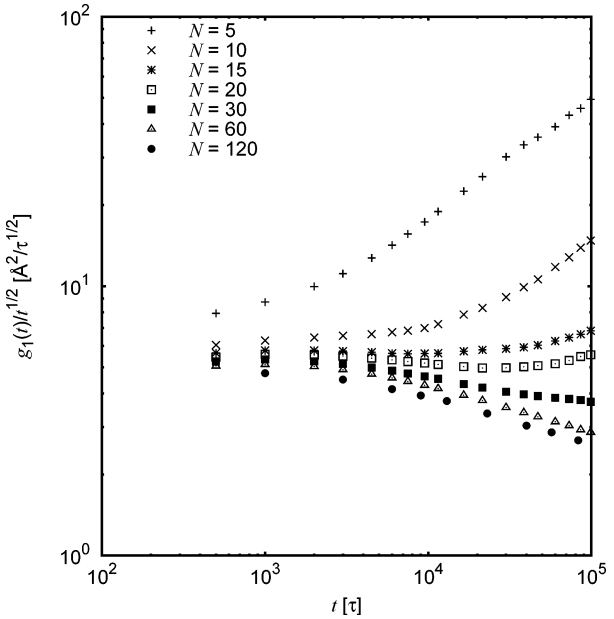

Figure 12. Variation of the ratio $g_1(t)/t^{1/2}$ vs t for the BPA-PC melts, showing the region where the Rouse regime takes place (power law exponent equal to 0).

Table 2. Time Shifts Used To Scale the Time When the Time−Temperature Superposition Principle Has Been Applied for g_1[a]

$4N + 3$	time shift for inner beads	$4N + 3$	time shift for inner beads
23	2.34	123	1.10
43	1.49	243	1.00
63	1.22	483	0.94
83	1.15		

[a] Because of the different accuracy of the individual simulation data, the system with the longest simulation time, $N = 60$, has been chosen as reference.

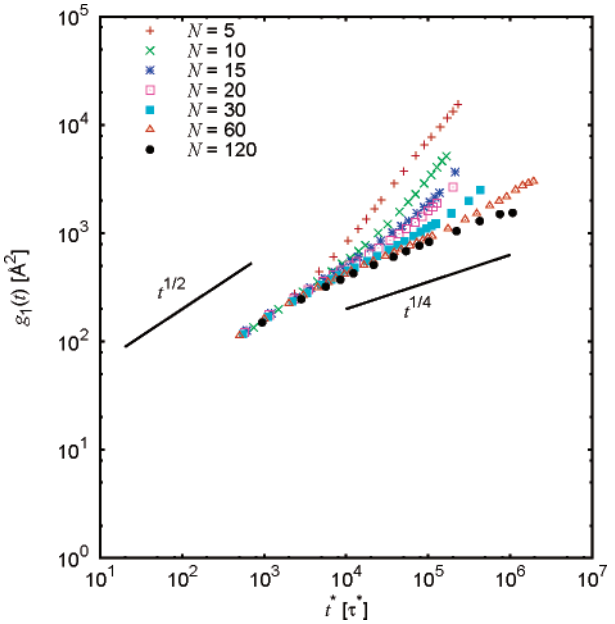

Figure 13. Scaled mean-squared displacement $g_1(t)$ for the inner beads for the BPA-PC melts, after the time−temperature superposition principle has been applied; this has been done by scaling t (now designated t^*) in the short time regime. Solid lines indicate the power law dependence of 1/2 and 1/4.

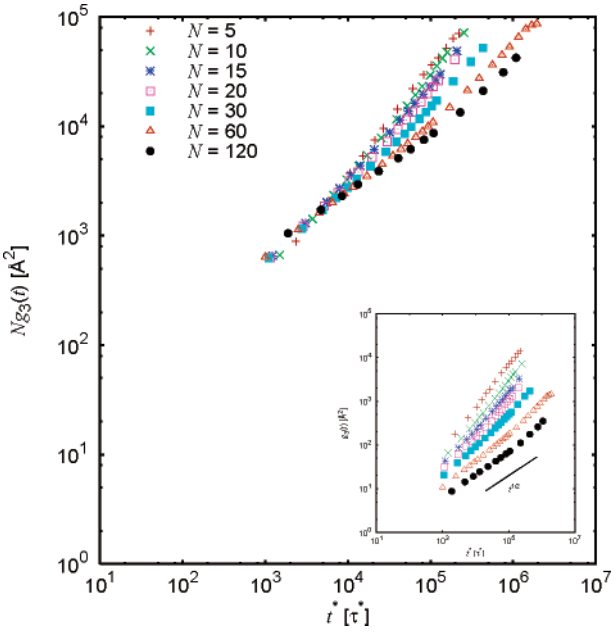

Figure 14. Mean-squared displacement g_3 scaled by the chain length N after the time−temperature superposition principle has been applied; this has been done by scaling t (now designated t^*) in the short time regime. The inset shows the same without the scaling by N; the solid line indicates the power law dependence of 1/2.

coincide when g_3 is scaled by the chain length N, as illustrated in Figure 14 (the nonscaled g_3 is shown as an inset in the same figure). The agreement is quite reasonable, however not as good as for g_1, because in the analysis only inner beads were used, while g_3 naturally averages over all beads. Using g_3 would have led to a slightly different rescaling. Employing the corrected g_1 and g_3, we now can estimate the entanglement length N_e.

C. Estimate for $N_{e,msd}$ and $N_{e,D}$ from Monomer and Chain Displacements. There are different ways

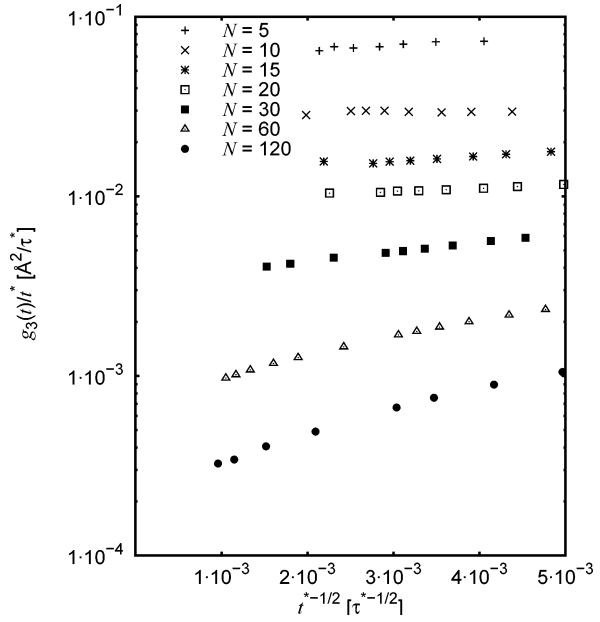

Figure 15. Variation of the ratio g_3/t^* vs $t^{*-1/2}$ (where t^* refers to the scaled time after the time−temperature superposition principle has been applied). Extrapolation of the value of g_3/t^* for $(t^{*-1/2}) \rightarrow 0$ provides the value of the self-diffusion coefficient D. Data are only shown for times where the error bar typically does not exceed the symbol size significantly.

to deduce a value for the entanglement length N_e from the mean-square displacements of the individual monomers $g_1(t)$ or the diffusion of the whole chain $g_3(t)$. To use the different crossover times (cf. eqs 13 and 14) is difficult because the prefactors are not exactly known and require some additional assumptions. In addition, τ_d is known to follow an $N^{3.4}$ power law rather than the predicted N^3 power law for all chain lengths typically employed in experiments and in simulations. This is due to a very slow crossover into the asymptotic regime.[35] One first unambiguous estimate of N_e results from the ratio $\tau_e/\tau_R \sim N_e^2/N^2$. Taking the two longest chain lengths and estimating $\tau_R(N)$ from $g_3(t)$ and τ_e from $g_1(t)$ according to eqs 13 and 14, we get a first estimate of $N_e \approx 8.5 \pm 3$. A more direct way is to look at the value of $g_1(t)$ at the crossover from the Rouse-like $t^{1/2}$ to the reptation $t^{1/4}$ regime. This is also open for some discussion, as the relation between $g_1(\tau_e)$, d_T, and N_e assumes perfect random walk properties of the chains already on that length scale. Figure 13 allows, based on the data for $N = 120$, to estimate $\tau_e \approx 1.0 \times 10^4\tau$ and $g_1(\tau_e) \approx 480 \pm 30$ Å^2. Assuming that up to then the beads of the chain followed an isotropic Rouse motion, we can estimate $g_1(\tau_e) = 2R_G^2(N_e)$. Taking the results of Figure 4 and Table 1, we find $N_e \approx 7$. Using the expression of the Rouse model incorporating directly the bead friction (see below) from Figure 9 and ref 22 gives $N_e \approx 6$. Thus, this all suggests a value of $N_{e,msd}$ between 6 and 9.

From the long time behavior of the scaled g_3, the value of the self-diffusion coefficient of the chains D can be obtained, via $g_3(t) = 6Dt$. This is shown in Figure 15, where the ratio g_3/t^* is given as a function of $1/t^{*1/2}$ for the different melts. The extrapolation of g_3/t^* vs $1/t^{*1/2}$ to $t^* \rightarrow \infty$ provides the diffusion coefficient D^* (the index refers to the fact that the time−temperature superposition principle has been applied). Such an extrapolation however bears some problems, as long as g_3/t^* did not reach a constant value. This is here somehow the case for $N = 60$ and 120. Thus, in Table 3 for these chain

Table 3. Total Time of the Simulations in Units of [τ] as Well as [s], Diffusion Constant $D^*(N)$ Obtained from the Scaled g_1 after the Time−Temperature Superposition Principle Has Been Applied, the Corresponding Scaled Diffusion Constant $D^*(N)/D_R^*(N)$, Diffusion Constant $D_0(N)$ Obtained without Application of the Time−Temperature Superposition Principle, and the Corresponding Scaled Diffusion Constant $D_0(N)/D_{0,R}(N)$[a]

N	simul time [τ]	simul time [s]	$6D^*(N)$ [[Å^2/τ]	$D^*(N)/D_R^*(N)$	$6D_0(N)$	$D_0(N)/D_{0,R}(N)$
5	100 000	2.6×10^{-6}	6.7×10^{-2}	1.00	1.6×10^{-1}	1.00
10	170 000	4.4×10^{-6}	2.9×10^{-2}	0.86	4.3×10^{-2}	0.55
15	210 000	5.46×10^{-6}	1.6×10^{-2}	0.73	1.9×10^{-2}	0.37
20	260 000	6.76×10^{-6}	1.1×10^{-2}	0.64	1.2×10^{-2}	0.31
30	460 000	1.2×10^{-5}	4×10^{-3}	0.35	4.4×10^{-3}	0.16
60	2 040 000	5.3×10^{-5}	$(6-7) \times 10^{-4}$	0.12	$(6-7) \times 10^{-4}$	5.0×10^{-2}
120	1 180 000	3.07×10^{-5}	$(2-3) \times 10^{-4}$	8.8×10^{-2}	$(2-3) \times 10^{-4}$	3.5×10^{-2}

[a] Note that the time values for the run times in units of [s], which are given for $T = 570$ K, will increase for $T = 500$ K by a factor of about 30 and for $T = 450$ K by a factor of about 33 200, respectively!

lengths we give the two limits for D^*, namely the linear extrapolation of the data to $t^* \to \infty$, which results in a value lower than $6D^*(N)$, and the last calculated value of g_3/t^*, which is larger than $6D^*(N)$ (cf. eq 14). All values obtained for D^* are summarized in Table 3.

It is known that the dependence of D with the chain length N is $D \sim 1/N$ for chains shorter than N_e (Rouse behavior) and $D \sim 1/N^2$ for longer chains (reptation behavior). Recent experiments[36,37] suggest an $N^{-2.5}$ power law, which would in a better way fit to the scaling of the viscosity $\eta \propto N^{3.4}$. On the other hand, an alternative theoretical concept for the crossover from Rouse to the fully entangled regime[39] claims a steeper slope only for $N \leq 10N_e$. The present data certainly are not in a regime $N \gg 10N_e$ to settle this. It has been shown by a comparison of simulations and experiments that the scaled diffusion coefficient $D(N)/D_R(N)$, with $D_R(N)$ being the (hypothetical) Rouse diffusion coefficient, to good accuracy is a universal function of the ratio N/N_e.[4] This provides a second way to estimate the entanglement length $N_{e,D}$ of BPA-PC from the calculation of the diffusion coefficient D. The Rouse diffusion coefficient $D_R(N)$ can be estimated from the diffusion coefficient of the shortest chain ($N = 5$), since

$$D_R(N) = \frac{k_B T}{\zeta(4N+3)} \tag{15}$$

where $\zeta = 75.6\tau^{*-1}$ is the bead friction and has to be multiplied by a factor 4 to give the characteristic monomeric coefficient. Plotting the so-determined scaled diffusion constant $D(N)/D_R(N)$ vs N/N_e, or $(4N+3)/4N_e$ for our 4:1 mapping scheme, giving $\approx 3.9\tau^{*-1}$ when the distance is measured in Å instead of σ, in one figure together with other published data[4] allows to obtain a fit for N_e, as shown in Figure 16. The resulting value of $N_{e,D} \approx 15 \pm 2$ chemical repeat units fits the comparison to other systems quite well, while it is rather different to the estimate from $g_1(t)$. At this point we can make another link to experiments. Using the value of D as given in Table 3, we can extrapolate to the diffusion of a single chemical repeat unit, D_{mon} (again using the bead representation). From $D(N = 5)$ we find $D_{mon} \approx D(N = 5) \times (4N+3)/4 = 6.4 \times 10^{-2}$ Å$^2/\tau$, which in real time units (within the huge uncertainty) leads to $D_{mon} \approx 2.5 \times 10^{-7}$ cm^2/s. This is somewhat more than 10 times slower than the diffusion of phenol in BPA-PC at the same temperature determined by all-atom simulations.[38]

D. Estimate of $N_{e,Sf}$ from the Dynamic Structure Factor. While the direct determination of intermediate mean-square displacements only recently became possible by e.g. NMR spectroscopy[40] and some very new

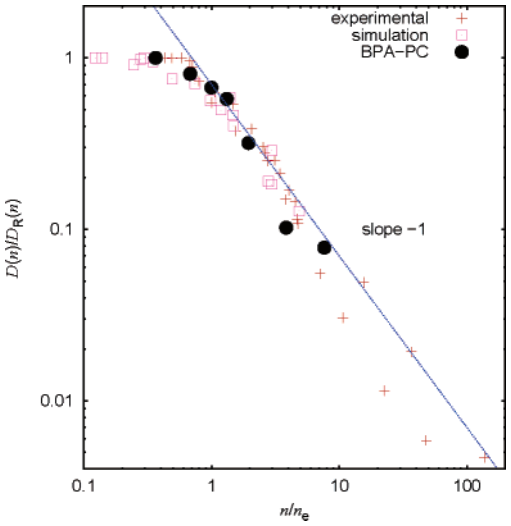

Figure 16. Scaled diffusion constant $D(n)/D_R(n)$ for the present BPA-PC data and $D(N)/D_R(N)$ for the reference data as a function of the scaled chain length n/n_e and N/N_e, respectively, from different experimental and simulation results for various polymer systems (data taken from ref 4). The best fit for the entanglement length yields $n_e = 62 \pm 8$ coarse-grained beads, giving approximately $N_{e,D} \simeq 15$.

neutron scattering data,[41] the time-dependent dynamic structure factor $S(q,t)$ of the chains has been studied for many years by neutron spin echo (NSE) spectroscopy.[42] This provides a complementary way to determine the tube diameter d_T and thus N_e. The dynamic single-chain structure factor $S(q,t)$ for the present model is defined as

$$S(q,t) = \frac{1}{4N+3}\left\langle \sum_{i,j} \exp[i\mathbf{q}\cdot(\mathbf{r}_i(t) - \mathbf{r}_j(0))] \right\rangle_{|\mathbf{q}|} \tag{16}$$

where the index $|\mathbf{q}|$ denotes the spherical average over all $\mathbf{q}$ directions. For the appropriate time ($t \ll \tau_d$) and q-space regime ($2\pi/R_G < q < 2\pi/d_T$), the dynamic structure factor can be expressed in the following way:[4,43,45]

$$\frac{S(q,t)}{S(q,0)} = \left\{\left[1 - \exp\left[-\left(\frac{qd_T}{6}\right)^2\right]\right] f\left(q^2 b^2 \sqrt{\frac{12Wt}{\pi}}\right) + \exp\left[-\left(\frac{qd_T}{6}\right)^2\right]\right\} \frac{8}{\pi^2} \sum_{p=1,\text{odd}}^{\infty} \frac{\exp\left[-\frac{tp^2}{\tau_d}\right]}{p^2} \tag{17}$$

where $f(u) = \exp[u^2/36]\ \mathrm{erf}(u/6)$. Since here $t \ll \tau_d$, the

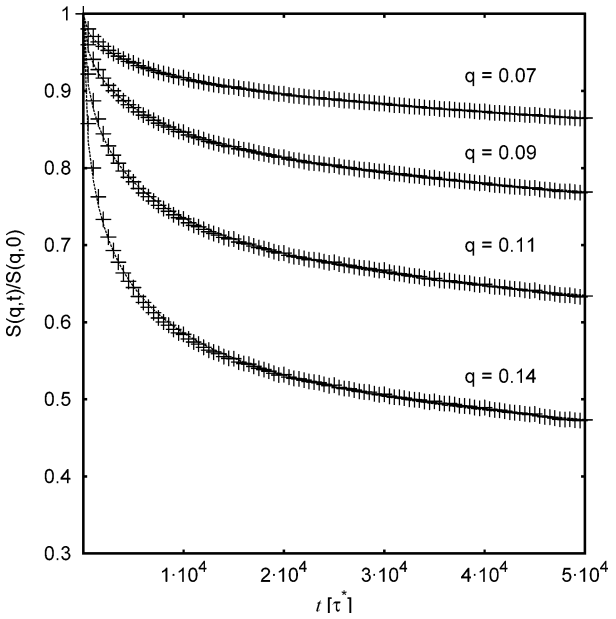

Figure 17. Scaled dynamic structure factor $S(q,t)/S(q,0)$ as a function of time for the melt with chain length $N = 120$ repeat units. For each q value, dotted lines show the fit to the expression of eq 17. Note that these curves are obtained for $4N + 3 = 483$ scattering beads per chain.

correction factor due to creep of the whole chain along the tube $[(8/\pi^2)\sum_{p=1,\text{odd}}^{\infty}(\exp(-tp^2/\tau_d)/p^2)]$ can be set to one. Within the picture provided by the reptation model the dynamic structure factor "samples" for the above time and q regime a region corresponding to the "tube" and observes the smeared out position of the beads. Accordingly, the corresponding tube diameter d_T can be estimated from a fit of eq 17 to the data, as shown in Figure 17. For this d_T and $b^2\sqrt{12W/\pi}$ have been fitted independently to each curve. The results for $b^2\sqrt{12W/\pi}$ range from $0.22\sigma^2\tau^{-1/2}$ to $0.29\sigma^2\tau^{-1/2}$ where each bead counts as a scatters. Within the description of the Rouse model, which is supposed to be applicable for the motion constrained to the tube regime in the reptation case, one can deduce from this the bead friction as well. Using $W = k_BT/\zeta b^2$ with $\langle R_{e-e}^2\rangle = b^2(4N + 3)$, which lead to $b^2 \approx 2.7\sigma^2$, one arrives at a bead friction between $\zeta = 122.6\tau^{*-1}$ from $b^2\sqrt{12W/\pi} = 0.29$ for $q = 0.07$ Å^{-1} and $\zeta = 213\tau^{*-1}$ for $b^2\sqrt{12W/\pi} = 0.22$ for $q = 0.14$ Å^{-1}, significantly above the value from the (very) short chain diffusion. One should however keep in mind that an enhancement of ζ has to be expected rather than a reduction[25,46] because of the longer chains employed. What is however somewhat surprising and not understood is that the larger friction is obtained for the larger q value. Next assuming that the $d_T^2 = R_{e-e}^2(N_e)$ hypothesis is valid,[25] it is possible to obtain the entanglement length N_e.

Figure 17 shows the structure factor for the melt with chains of $N = 120$ repeat units for q ranging from 0.07 to 0.14 Å^{-1}. d_T from fits to eq 17 for each q value are in Table 4. The different values for d_T and N_e vary only weakly for different q values, providing an estimated entanglement length $N_{e,sf}$ from the dynamic structure factor around 10 repeat units. For melts of shorter chains, however, the results are not so clear. These chains are probably too short in terms of the number of entanglements; in particular, larger values for both d_T and N_e and in a wider range are obtained. (For example, for $N = 60$, the resulting N_e ranges from 12 to 18 repeat units. The reason most probably comes from the problem that for such a short chain R_G is not significantly larger than the tube diameter d_T.)

Table 4. Estimated Values of the Tube Diameter d_T (Å) and the Entanglement Length $N_{e,sf}$ Obtained from the Fitting of the Calculated Dynamic Structure Factor for the Melt with $N = 120$ to the Expression of Eq 17[a]

q value	$d_T(q)$	$N_{e,sf}(q)$
0.07	46.6	10.3
0.09	46.4	10.3
0.11	45.8	10.0
0.14	45.0	9.6

[a] The results are reported for each q value.

Experimentally in most cases the above expression of eq 17 is fitted simultaneously to the decay curves for all q values. Doing this for the present systems yields $b^2\sqrt{12W/\pi} = 0.276$ and $d_T = 43.4$ Å, giving a slightly smaller value of $N_{e,sf}$ close to 9 repeat units. The fit to the whole data set is almost as good as for the individual data sets with the characteristic weakly faster decay for short times for the larger q values and a corresponding slower decay for longer times for the smaller q values, just as found in experiment.[42−44] The separate analysis, however, reveals in more detail the potential problems, which are hidden in the analysis of $S(q,t)$ to determine N_e.

E. Estimate of $N_{e,pm}$ from the Plateau Modulus. Originally the reptation or tube concept was developed to understand the similarity in the stress relaxation of long chain polymer networks and long chain polymer melts. The tube diameter, and with that N_e, for the dynamic confinement of the chains is the unique parameter, which describes the modulus. Thus, another, or the "original", way to obtain the entanglement length N_e experimentally is by the determination of the plateau modulus G_N^0. There usually an oscillatory shear is applied to determine the real and the imaginary part of the modulus G. This is also the area, where the time−temperature superposition is typically employed in order to extend the dynamic range of the rheometers. Here we follow a slightly different route. In the simulation a volume conserving step strain elongation for two different amplitudes $\lambda = 1.25$ and 1.50 is applied to the melts. The time-dependent normal stresses $\sigma_N(t)$ were determined by the microscopic virial tensor.[4] The plateau values $\sigma_N = \lim_{\tau_e \ll t \ll \tau_d}\sigma_N(t)$ were fitted to the stress−strain formulas for classical rubber elasticity (CRE)[47]

$$\sigma_N = G_N^0\left(\lambda^2 - \frac{1}{\lambda}\right) \tag{18}$$

and to the Mooney−Rivlin formula (MR)[49]

$$\begin{aligned}\sigma_N &= 2G_1\left(\lambda^2 - \frac{1}{\lambda}\right) + 2G_2\left(\lambda - \frac{1}{\lambda^2}\right)\\ &= 2(G_1 + G_2/\lambda)\left(\lambda^2 - \frac{1}{\lambda}\right)\end{aligned} \tag{19}$$

G_N^0 in turn is related to the entanglement length N_e[1,48] via the expression

$$G_N^0 = \frac{4}{5}\frac{\rho k_BT}{4N_e} \tag{20}$$

Here we again have to use $4N_e$ since each chemical

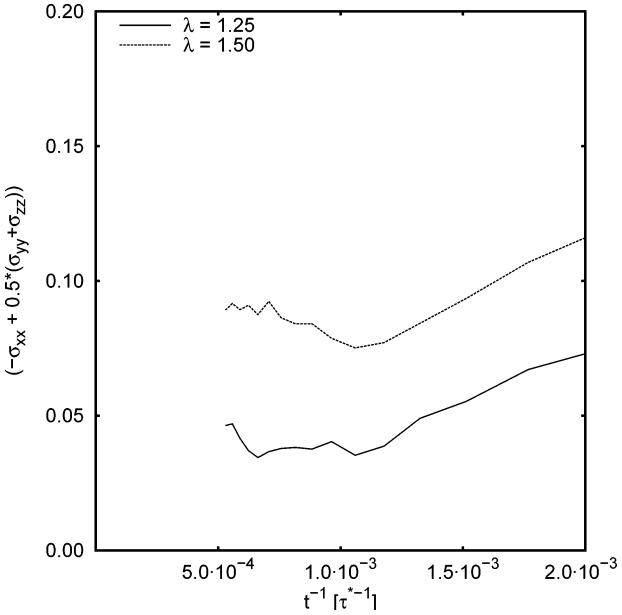

Figure 18. Variation of the tension as a function of the inverse of time, for the BPA-PC melt with $N = 120$ repeat units, giving $4N + 3 = 483$ beads per chain, for elongations $\lambda = 1.25$ and 1.50.

Table 5. Estimated Values of the Tension σ_N, the Plateau Modulus $G^0_{N,\mathrm{pm}}$, and the Entanglement Length $N_{\mathrm{e,pm}}$ Obtained from Relaxation Simulations on BPA-PC Melts with $N = 120$ Repeat Units and Elongation $\lambda = 1.25$ and 1.50[a]

formula	λ	σ_N	$G^0_{N,\mathrm{pm}}$	$N_{\mathrm{e},pm}$
CRE	1.25	0.035	0.045	3.7 ± 2
CRE	1.50	0.075	0.047	3.6 ± 2
MR			0.044	≈4

[a] Extrapolation of the CRE values for $\lambda = 1$ yields an $N_{\mathrm{e,pm}}$ between 5 and 6 repeat units.

repeat unit corresponds to four beads and the density, $\rho = 0.85\sigma^{-3}$, counts the beads, which does not correspond to the monomer density. Results obtained using both the CRE and the MR formulas for the melt with $N = 120$ for $\lambda = 1.25$ and 1.50 are summarized in Figure 18 and Table 5. While G^0_N is directly given by the CRE equation, it follows for the MR analysis from $G^0_N = 2(G_1 + G_2/\lambda)$ extrapolated to $\lambda = 1$. What is quite interesting is that the rubbery plateau develops already for times within the crossover from the first $t^{1/2}$ to the $t^{1/4}$ regime in $g_1(t)$, irrespectively of the strain applied. Taking the results of the time-dependent modulus, a value of the entanglement length $N_{\mathrm{e,pm}}$ from the plateau modulus around the very small value of 4 repeat units is obtained. Similar to the analysis of $S(q,t)$ only data for the longest chains provide a good estimate of $N_{\mathrm{e,pm}}$. No good extrapolation for σ_N can be made even for melts with $N = 60$ repeat units (the error bars are too large).

F. Estimate of $N_{\mathrm{e,pp}}$ from a Primitive Path Analysis. So far typical experimental quantities have been obtained and analyzed. Originally, the idea of Edwards was to link the modulus to the conformations and the chain−chain interpenetration within the melts. This link between the overall melt conformation and modulus has been established in a recently developed topology analysis, which allows to determine the primitive path of the chains and thus G^0 and N_e.[7] There it has been shown that this leads to excellent predictions

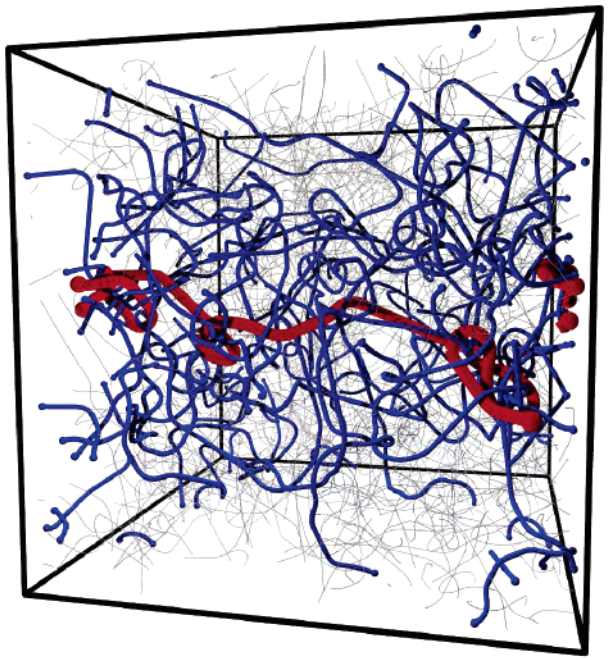

Figure 19. Result of the primitive path analysis for all chains in the melt of 100 chains of $N = 60$ repeat units (243 beads). We show the primitive path of one chain (red) together with all of those it is entangled with (blue). The primitive paths of all other chains in the system are shown as thin lines.

of the modulus and compares very well to a variety of systems covering about 6 decades in properly normalized moduli, including BPA-PC. This analysis is adopted here and carried out for the different systems in the following way: first, the chain ends are fixed in space, and the intrachain excluded-volume interactions are switched off, while retaining the interchain excluded-volume interactions. Then the energy of the system is minimized by slowly cooling the system to $T = 0$ K. Without thermal fluctuations and intrachain excluded-volume interactions, the bond springs try to reduce the bond lengths to zero, while interchain excluded-volume interactions ensure that the topological constraints are conserved. Such a procedure results in a mesh of primitive paths as illustrated in Figure 19; for details of the procedure we refer to refs 7 and 8. A recent extension of that algorithm to include self-entanglements[8] shows that they on the present level of accuracy are irrelevant and can be neglected.

The primitive path analysis has been applied to all the BPA-PC melts studied in this work; in addition, melts with chain lengths as short as $N = 1$ and 2 repeat units have been also considered for comparison (note that these are, due to our mapping, 7 and 11 bead chains). Since $R_{\mathrm{e-e}}$ of both the primitive path and the original chains are the same, this procedure directly yields the Kuhn length a_{pp} of the primitive paths. Following refs 7 and 8 this determines the entanglement length via

$$N_{\mathrm{e}} = a_{\mathrm{pp}}{}^2 N/\langle R^2(N)\rangle \tag{21}$$

As in other cases, the lengths of the primitive paths and with this the effective $N_e(N)$ first grows linearly with the chain length, until it settles at the asymptotic value. Results are summarized in Table 6 and Figure 20. It can be seen that the estimated values for the longer melts are very similar to those obtained from the

Table 6. Values of the Plateau Modulus $G^0_{N,pp}$ and the Entanglement Length $N_{e,pp}$ Obtained from the Primitive Path Analysis on BPA-PC Melts[a]

N	$G^0_{N,pp}$	$N_{e,pp}$	N	$G^0_{N,pp}$	$N_{e,pp}$
1	0.142	1.19	20	0.033	5.13
2	0.093	1.84	30	0.029	5.91
5	0.052	3.25	60	0.031	5.48
10	0.040	4.28	120	0.031	5.47
15	0.038	4.51			

[a] Since the given values for each specific system are "exact", the uncertainty is best reproduced by the variation of the last three values.

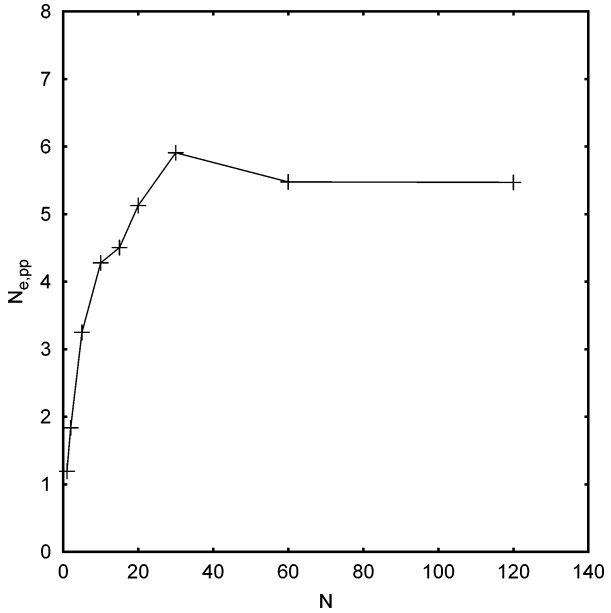

Figure 20. Variation of the entanglement length $N_{e,pp}$ obtained from the primitive path analysis with the chain length, for the melts with $N = 1$, 2, 5, 15, 20, 30, 60, and 120 repeat units.

direct numerical "elongation experiment" (compare Table 5 and Table 6), yielding a value of the entanglement length of $N_{e,pp}$ from the primitive path analysis of about 5−6. It should be remarked that the results of the primitive path analysis converge fast, indicating that reasonable values can be obtained for relatively short chain lengths, like $N = 20$−30 repeat units for BPA-PC. This provides a clear advantage of the primitive path analysis with respect to all other ways to estimate the entanglement length: for instance, the analysis of the dynamic structure factor or the determination of G^0_N only provide good results for the longest chain lengths!

IV. Conclusions

The different estimates of the entanglement length presented in this work show a significant spread, which is in accord with previous studies on simple bead−spring chains with variable flexibility.[4,5] On the other hand, taking the results from the primitive path analysis and the direct determination of the modulus, this fits well, as for all other polymers tested, into the general scaling scheme developed in refs 7 and 8. There BPA-PC was found to be close to the upper limit of the validity of the standard tube concept scheme (roughly spoken this is where the Kuhn length of the chain and d_T meet). Thus, the extraordinarily small entanglement length seems nothing special from that point of view. The results from the primitive path topology analysis provide a basis for a link between chain conformation, packing, and modulus. As it turns out, the construction of the primitive path simultaneously for all chains in the system leads to a value of N_e, which quantitatively is close to the results from the elastic modulus. In addition, it remarkably agrees with the finding that the modulus is proportional to p^{-3}, p being the so-called packing length.[6,7] What is however important to note is that the determination of N_e based on other quantities than the modulus or the topology does not necessarily give an answer at all that allows to predict the outcome of other experiments. This is illustrated by the summary of results from simulations in Table 7. The deviations easily reach a factor of 2.

The results of this work emphasize the problem that different experimental techniques might lead to rather different values for N_e. Unfortunately, there is no established relation between the value of N_e coming out of the mean-square displacements of the beads, diffusion constant $D(N)$, the intermediate single chain scattering function $S(q,t)$, and the plateau modulus G^0_N. The present data, as well as other simulation data,[4,5] do not give indications that the ratio or even the order between the different values remains the same. For the simple bead−spring chains, where the only variation came from an intrinsic stiffness, it is found that N_e determined from the modulus always is larger than that coming from the scattering function and the one obtained directly from the bead displacements. This order for

Table 7. Comparison of the Plateau Modulus G^0_N (MPa), the Entanglement Length N_e, and the Entanglement Weight M_e (g/mol) Obtained from Different Experimental Techniques at Different Temperature (K) and the Estimates Obtained in This Work

measurement	temp (K)	G^0_N	N_e	M_e	reference
			9.48	2400	11, 12
			11.81	3000	13
			7.87	2000	14
rheology			7.13	1810	15
oscillatory shear	462	2.00	8.58	2180	16
solution rheology	298		6.30	1600	6
rheology	487		5.2	1330	50
		1.20	9.84	2500	17
rheology	493		<5.8	<1480	51
mean-squared displacement	570		6−10	1524−2540	this work
diffusion coefficient	570		13−17	3800	this work
dynamic structure factor	570		10	2540	this work
elongation simulation	570	0.044−0.047[a]	≈4	≈1016	this work
primitive path analysis	570	0.031[a]	≈5.5	1389	this work

[a] In LJ units, which can be directly transformed into experimental analogues by using eq 20.

BPA-PC is reversed. Thus, measuring N_e from one quantity generally cannot be used to predict the result of a different experiment on the same sample! Taken the general concept of the theory, the result from the modulus should be be taken as "the" N_e value, which nicely agrees with the one calculated from the topological analysis.

Table 7 also includes the results from a number of different experiments. They, although most of the data come from rheology, also show a wide spread. Even taking into account that experiments were made at different temperatures, this spread is very large. However, this also displays a typical problem for experiments on (in most cases) commercial samples. BPA-PC usually is synthesized in a polycondensation process, which leads to a significant polydispersity. CD grade BPA-PC still has $M_w/M_n \approx 2.3$.[16] Taking the more recent original publications,[6,15,16,50] there is a clear tendency toward smaller values. Within this group the results on CD grade BPA-PC[16] give the largest N_e. However, there one has a huge polydispersity, which due to the presence of many very short chains "dilutes" the entanglement density. Thus, the typical experiments, which do not test especially fractionated monodisperse samples, only can give an upper limit for N_e of the pure substance. Unfortunately, in most papers neither M_w nor the polydispersity is given. There is one slightly different ansatz which tackles this problem from a different direction. In ref 51 a series of experiments with increasing M_w were performed. In the table the number for $M_w = 59\,000$ is given. The extrapolation to $M_w = \infty$ yields a value close to $N_e = 5$, in excellent agreement with the simulation results.

To summarize, the present study contains a rather exhaustive set of "measurements" of the entanglement length or molecular weight of BPA-PC. It in two ways reveals a significant advantage to typical experiments. First the set of different, typical experimental quantities is determined, and then also a topological conformational analysis is performed on exactly the same systems at one fixed temperature. This is not possible for experiments. A second advantage is that the simulated systems are absolutely monodisperse, i.e., $M_w/M_n = 1$. In other terms, our systems are perfectly characterized. Of course, polydispersity can be introduced at will at any time. With the increase of computer power combined with optimized algorithms and models this is possible nowadays.

Besides this, the present simulation study contains another significant step. By employing a suitably coarse-grained model of BPA-PC it was possible to follow the dynamics of a specific chemical melt of 200 chains of about $20N_e$ at the characteristic process temperature of $T = 570$ K for times up to about 10^{-4} s, several orders of longer than any other study before. The relaxation functions given can directly be compared to or used to predict experimental results, essentially without any adjustable parameter. Even beyond that, using a standard time−temperature superposition scheme as done in experiment (within the approximations and error estimate given), our simulations extend to times around 4×10^{-3} s for $T = 500$ K and even around 4 s for $T = 450$ K, a truly macroscopic time. We certainly will follow this route also for other polymers as well as more complicated topologies, where less detailed experiments are available.

Acknowledgment. We are grateful to S. Sukuraman and A. Sivasubramanian for their help with the primitive path analysis. We thank C. F. Abrams and F. Bruder for many discussions in the early stage of this work. The work was supported by the Bayer AG and the Bundesministerium für Bildung and Forschung (the German Federal Ministry of Education and Research), Grant 03 N 6015 on materials simulations.

References and Notes

(1) Doi, M.; Edwards, S. F. *The Theory of Polymer Dynamics*; Clarendon Press: Oxford, 1986.
(2) De Gennes, P.-G. *Scaling Concepts in Polymer Physics*; Cornell University Press: Ithaca, NY, 1979.
(3) Ferry, J. D. *Viscoelastic Properties of Polymers*; Wiley: New York, 1980.
(4) Pütz, M.; Kremer, K.; Grest, G. S. *Europhys. Lett.* **2000**, *49*, 735.
(5) Kremer, K.; Sukumaran, S. K.; Everaers, R.; Grest, G. S. *Comput. Phys. Commun.* **2005**, *169*, 75.
(6) Fetters, L. J.; Lohse, D. J.; Milner, S. T.; Graessley, W. W. *Macromolecules* **1999**, *32*, 6847.
(7) Evereaers, R.; Sukumaran, S. K.; Grest, G. S.; Svaneborg, C.; Sivasubramanian, A.; Kremer, K. *Science* **2004**, *303*, 823−826.
(8) Sukumaran, S. K.; Grest, G. S.; Kremer, K.; Everaers, R. *J. Polym. Sci., Polym. Phys.* **2005**, *43*, 917.
(9) Padding, J. T.; Briels, W. J. *J. Chem. Phys.* **2004**, *120*, 2996.
(10) Kröger, M.; Ramirez, J.; Oettinger, H. C. *Polymer* **2002**, *43*, 477. Kröger, M. *Comput. Phys. Commun.*, in press.
(11) Mercier, J. P.; Aklonis, J. J.; Litt, M.; Tobolsky, A. V. *J. Appl. Polym. Sci.* **1965**, *9*, 447.
(12) Prevorsek, D. C.; Debona, B. T. *J. Macromol. Sci., Phys. B* **1981**, *19*, 605.
(13) Prevorsek, D. C.; Debona, B. T. *J. Macromol. Sci., Phys. B* **1986**, *25*, 515.
(14) Wu, S. *Polym. Eng. Sci.* **1992**, *32*, 823.
(15) Plummer, C. J. G.; Soles, C. L.; Xiao, C.; Wu, J.; Kausch, H. H.; Yee, A. F. *Macromolecules* **1995**, *28*, 7157.
(16) Wimberger-Friedl, R.; Hut, M. G. T.; Schoo, H. F. M. *Macromolecules* **1996**, *29*, 5453.
(17) Jordan, T. C.; Richards, W. D. In *Handbook of Polycarbonate Science and Technology*; Legrand, D. G., Bendler, J. T., Eds.; New York, 2000; Chapter 9.
(18) Binder, K., Ed. *Monte Carlo and Molecular Dynamics Simulations in Polymer Science*; Oxford University Press: New York, 1995.
(19) Kremer, K. In *Monte Carlo and Molecular Dynamics of Condensed Matter Systems*; Binder, K., Ciccotti, G., Eds.; Italian Phys. Soc.: Bologna, 1996.
(20) Kremer, K. In *Computational Soft Matter: From Synthetic Polymers to Proteins*; Attig, N., Binder, K., Grubmüller, H., Kremer, K., Eds.; NIC Lecture Notes 23; Jülich, 2004.
(21) Tschöp, W.; Kremer, K.; Batoulis, J.; Bürger, T.; Hahn, O. *Acta Polym.* **1998**, *49*, 61.
(22) Abrams, C. F.; Kremer, K. *Macromolecules* **2003**, *36*, 260−267. (Note that the data for the friction coefficients in Table 3 of that paper are given per bead and for displacements measured in σ.)
(23) Abrams, C. F.; Delle Site, L.; Kremer, K. *Phys. Rev. E* **2003**, *67*, 021807.
(24) Sanchez, I. C.; Cho, J. *Polymer* **1995**, *36*, 2929.
(25) Kremer, K.; Grest, G. S. *J. Chem. Phys.* **1990**, *92*, 5057.
(26) Abrams, C. F.; Kremer, K. *J. Chem. Phys.* **2001**, *115*, 2776.
(27) Eilhard, J.; Zirkel, A.; Tschöp, W.; Hahn, O.; Kremer, K.; Schärpf, O.; Richter, D.; Buchenau, U. *J. Chem. Phys.* **1999**, *110*, 1819.
(28) Auhl, R.; Everaers, R.; Grest, G. S.; Kremer, K.; Plimpton, S. J. *J. Chem. Phys.* **2003**, *119*, 12718.
(29) Eilhard, J. In *Untersuchungen zur Struktur und Dynamic von Polykondensaten*; Jül-Bericht: Jülich, Germany, 1996.
(30) Moore, V. R.; Uddin, M. A. *Eur. Polym. J.* **1970**, *6*, 121.
(31) Paul, W.; Smith, G. D. *Rep. Prog. Phys.* **2004**, *67*, 1117.
(32) Guenza, M. *Phys. Rev. Lett.* **2002**, *88*, 025901.
(33) Macosko, C. In *Rheology: Principles, Measurements and Applications*; Wiley-VCH: New York, 1994.
(34) Paul, W. *Chem. Phys.* **2002**, *284*, 59.
(35) Pearson, D. S.; Fetters, L. J.; Graessley, W. W.; Strate, G. V.; von Meerwall, E. *Macromolecules* **1994**, *27*, 711.
(36) Lodge, T. P. *Phys. Rev. Lett.* **1999**, *83*, 3218.

(37) Tao, H.; Lodge, T. P.; von Meerwall, E. D. *Macromolecules* **2000**, *33*, 1747.
(38) Hahn, O.; Mooney, D. A.; Müller-Plathe, F.; Kremer, K. *J. Chem. Phys.* **1999**, *111*, 6061.
(39) Pokrovskii, V. N. *Adv. Polym. Sci.* **2001**, *154*, 143. Altukhov, Y. A.; Pokrovskii, V. N.; Pyshnograi, G. V. *J. Non-Newtonian Fluid Mech.* **2004**, *121*, 73.
(40) Graf, R.; Heuer, A.; Spiess, H. W. *Phys. Rev. Lett.* **1998**, *80*, 5738. Komlosh, M. E.; Callaghan, P. T. *J. Chem. Phys.* **1998**, *109*, 10053. Pahl, S.; Fleischer, G.; Fujara, F.; Geil, B. *Macromolecules* **1997**, *30*, 1414.
(41) Monkenbusch, M.; Wischnewski, A.; Willner, L.; Richter, D. *Physica B* **2004**, *350*, 214.
(42) Richter, D.; Ewen, B. *Adv. Polym. Sci.* **1997**, *134*, 1.
(43) Schleger, P.; Farago, B.; Lartigue, C.; Kollmar, A.; Richter, D. *Phys. Rev. Lett.* **1998**, *81*, 124.
(44) Wischnewski, A.; Richter, D.; Monkenbusch, M.; Willner, L.; Farago, B.; Ehlers, G.; Schleger, P. *Physica B* **2000**, *276*, 337.
(45) Kremer, K.; Binder, K. *J. Chem. Phys.* **1984**, *81*, 6381.
(46) Kreer, T.; Baschnagel, J.; Müller, M.; Binder, K. *Macromolecules* **2001**, *34*, 1105.
(47) Treloar, L. R. G. In *The Physics of Rubber Elasticity*; Clarendon Press: Oxford, 1986.
(48) Doi, M. *J. Polym. Sci.* **1980**, *18*, 1005.
(49) Mooney, M. *J. Appl. Phys.* **1940**, *11*, 582.
(50) Fetters, L. J.; Lohse, D. J.; Richter, D.; Witten, T. A.; Zirkel, A. *Macromolecules* **1994**, *27*, 4639.
(51) Bruder, F.; Bayer, A. G., private communication, 2004.
(52) In refs 22 and 23, an incorrect value of 4.49 Å is given.
(53) Note, however, that a misprint occurred in Tables 3 and 4 of refs 21 and 27, where a conversion factor in terms of Å/σ, instead of Å^2/σ^2, was used, so comparison of $\langle R_{e-e}^2 \rangle$ and $\langle R_G^2 \rangle$ with this work has to be made with caution.

MA050943M